Synthesis and characterization of a new hydrazone-coumarin chemosensor for Fe^{3+} in a water-acetonitrile mixture

Simeon Shiweda Hamukoshi,[a]* Neliswa Mama,[a] Jean Marie Vianney Ngororabanga,[b] Stiaan Schoeman,[a] Natangue Heita Shafuda,[c] Veikko Uahengo,[c] and Eric Hosten[a]

[a]Department of Chemistry, Nelson Mandela University, Port Elizabeth, South Africa. [b]Department of Mathematics, Sciences and Physical Education, University of Rwanda College of Education, Rwamagana-Eastern province, Rwanda. [c]Department of Physics, Chemistry and Materials Science, Faculty of Agriculture, Engineering and Natural Sciences, University of Namibia, Windhoek, Namibia
*Email: s218169809@mandela.ac.za*

Abstract

A new coumarin-based fluorescent chemosensor, **3**, incorporating a hydrazone (-NH-N=C-), was designed and synthesized. The chemosensor displayed higher affinity towards Fe^{3+} in water-acetonitrile solution in the presence of other competing cations in emission and absorption essays. The binding stoichiometry between the chemosensor **3** and Fe^{3+} was shown to occur in a 1:1 ratio, and the binding modes of the chemosensor towards Fe^{3+} were identified through the emission response, ^{1}H NMR, FT-IR and molecular modelling studies. The hydroxyl and amine functionalities on **3** were recognized as possible binding sites. The chemosensor presented a limit of detection, a limit of quantification and the association constant of 0.45 μM, 1.50 μM and 3.01 × 10^1 M^{-1}, respectively.

Highly Fluorescent **3**   Quenched Fluorescent **3**
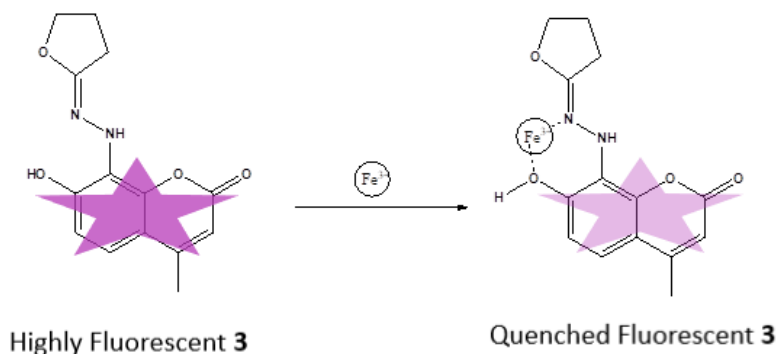
Keywords: Coumarin, fluorescent, chemosensor, molecular modelling

Introduction

Iron is the second most abundant heavy metal on Earth [1]. It is an essential heavy metal in the human body, playing a crucial role in complex formation with proteins and enzymes that facilitate important physiological processes, including oxygen binding and participation in the electron transport chain [2-3]. However, excessive iron can be toxic to humans and other living organisms [4]. When free iron accumulates in the liver, heart, and nervous system, it enters cells and causes damage to mitochondria [5]. This interruption of vital cellular mechanisms leads to the formation of radicals, ultimately resulting in cell death [6-7]. The presence of ferric ions in the environment is mainly attributed to natural resources and human activities such as mining [8], as well as industrial [9] or municipal wastewater [10], which subsequently contaminate soil, vegetation, and water [11]. In developing communities, ferric ions may contaminate drinking water through pipe corrosion. The World Health Organization (WHO) regulations recommend a ferric ion dose of 0.3 mg/L in drinking water, although this may slightly vary depending on the geographical location and coagulating agents used in water treatment plants [12]. Monitoring the concentration of Fe^{3+} in drinking water is crucial for the preservation of public health. Water purification facilities commonly employ spectroscopy techniques, such as atomic absorption spectroscopy (AAS)[13], inductively coupled plasma-mass spectrometry (ICP-MS) [14], cold-vapor atomic fluorescence spectroscopy (CV-AFS) [15], and neutron activation analysis (NAA) [16], to quantitatively monitor iron levels in water. However, these techniques are expensive, destructive, and highly labor-intensive [17-18]. Additionally, they require sophisticated instrumentation unsuitable for field use, skilled personnel, complicated sample collection, pre-treatment, and long measurement periods [19].Optical sensors, including colorimetric and fluorometric chemosensors, utilize electromagnetic radiation to detect analytes across a broad range of wavelengths [20,21]. These sensors employ principles such as absorbance, reflectance, fluorescence, and phosphorescence to measure the properties of light and determine the presence of analytes. Comprising a synthetic binding site, a chromophore or fluorophore, and mechanisms for modifying optical properties upon analyte binding, these sensors offer stability and can be tailored for diverse analytes, unlike biological receptors. Optical sensors provide several advantages over conventional analytical methods, including enhanced sensitivity, selectivity, and the capability to operate across different wavelengths [22]. Several small molecule fluorescent sensors have been developed to detect Fe^{3+} [23-24]. However, many of these sensors still face challenges such as poor selectivity, weak sensitivity, and low water solubility. Typically, fluorescent molecular sensors consist of a receptor unit chemically bonded to a light-emitting chromogenic or electrochemical fluorophore or recognition unit. The sensitivity of the recognition unit towards a specific analyte characterizes molecular sensors [25]. Recent studies indicate that fluorescent chemosensors incorporating a coumarin motif as a recognition unit, along with ligands attached to their core, can address issues such as poor metal ion selectivity and sensitivity [26]. This is attributed to the coumarin molecule's sensitivity, high quantum yield, ease of synthesis, and structural tunability of the conjugated coumarin motif [27-28]. Additionally, hydroxyl functionalities have also been reported to enhance the hydrophilic properties of the coumarin backbone [29][30][31]. Quang et al. developed a chemodosimeter based on a rhodamine-6G Schiff base for the selective detection of Fe^{3+} ions. Upon the addition of Fe(III) ions to an aqueous solution, the chemosensor demonstrated a significant enhancement in fluorescence. This study not only showcased the high selectivity of the chemosensor towards Fe^{3+} ions but also highlighted its potential application in monitoring Fe(III) levels in living cells [32]. In a separate investigation, Zhang et al. presented a cation sensor with the capability of specifically detecting Fe^{3+} ions even in the presence of other metal ions [33]. The sensor design was characterized by its simplicity and its ability to achieve remarkable sensitivity and selectivity towards Fe3+ ions. Additionally, Luo and colleagues designed a colorimetric chemosensor based on bis-(rhodamine) for the recognition of trivalent ferric ions (Fe3+). The chemosensor exhibited exceptional selectivity

and sensitivity towards Fe^{3+} ions [34].Top of Form Furthermore, several other Fe3+ chemosensors have been reported and discussed in the literature [35–38].

    Building upon the aforementioned research and our investigation into fluorescent colorimetric chemosensors [39–45], this study introduces a novel coumarin derivative bearing a hydrazone moiety, namely (E)-8-(2-(dihydrofuran-2(3H)-ylidene)hydrazinyl)-7-hydroxy-4-methyl-2H-chromen-2-one (3). The incorporation of nitrogen groups in the hydrazone and the lone pairs of the hydroxyl group provides specific binding sites for Fe^{3+}. Chemosensor **3** exhibits a strong affinity towards Fe^{3+} ions, even in the presence of other commonly occurring metal ions in water-acetonitrile solutions, via a turn-off fluorescence mechanism.
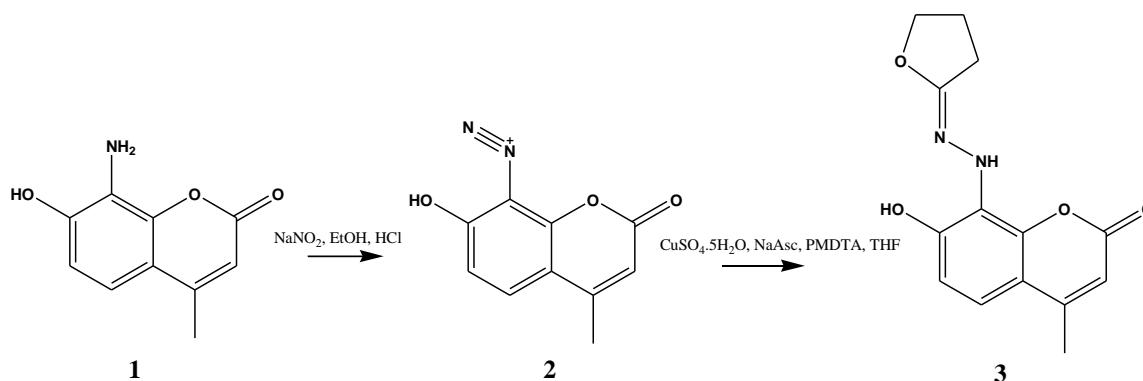
Results and Discussion

Synthesis of (*E*)-8-(2-(dihydrofuran-2(3*H*) ylidene)hydrazinyl)-7-hydroxy-4-methyl-2*H*-chromen-2-one (3)
The study commenced with the synthesis of fluorescent coumarin-containing hydrazone compound **3**. The synthesis of compound **3** involved a series of multi-step reactions starting from resorcinol. Initially, 37 g of resorcinol was dissolved in 45 ml of ethyl acetoacetate, and the resulting solution was slowly added to a cold 150 ml solution of H_2SO_4 while carefully maintaining the temperature below 10°C. The mixture was stirred for 0.5 hours, followed by its pouring into ice-cold water. Subsequently, the solid product, 7-hydroxy-4-methyl-2H-chromen-2-one, was isolated by filtration and drying.In parallel, coumarin derivative **1** was prepared using established procedures described in the literature[46-47]. The synthesis of coumarin derivative **1** involved a two-step process starting from resorcinol. By employing these multiple-step syntheses, various coumarin derivatives were generated as intermediates, ultimately leading to the synthesis of the target fluorescent coumarin-containing hydrazone compound **3**.
Top of Form
Bottom of Form

Scheme 1. Reaction scheme for the synthesis of (*E*)-8-(2-(dihydrofuran-2(3*H*)-ylidene)hydrazinyl)-7-hydroxy-4-methyl-*2H*-chromen-2-one (**3**).

X-Ray structure of 3

Further structure confirmation of chemosensor **3** was done using single-crystal X-ray diffraction analysis. Compound **3** was recrystallized in THF solvent to afford suitable crystals for x-ray studies. The single-crystal structure for chemosensor **3** (Figure 1B) is presented as expected, with the coumarin ring and all substituents in the same plane. However, there is a difference in the orientation of the tetrahydrofuran ring in the X-ray structure to that of the computational structure of **3** (Figure 1C). This is because the crystal structure was obtained in its fixed solid state, whereas the computational structure was in its gas state. Otherwise, all the substituents and functionalities of **3** are presented on the crystal structure. Hydrogen bonding was observed to stabilize **3** through the hydroxyl group at position 7 of the coumarin and the imine nitrogen, connected to the furan ring.
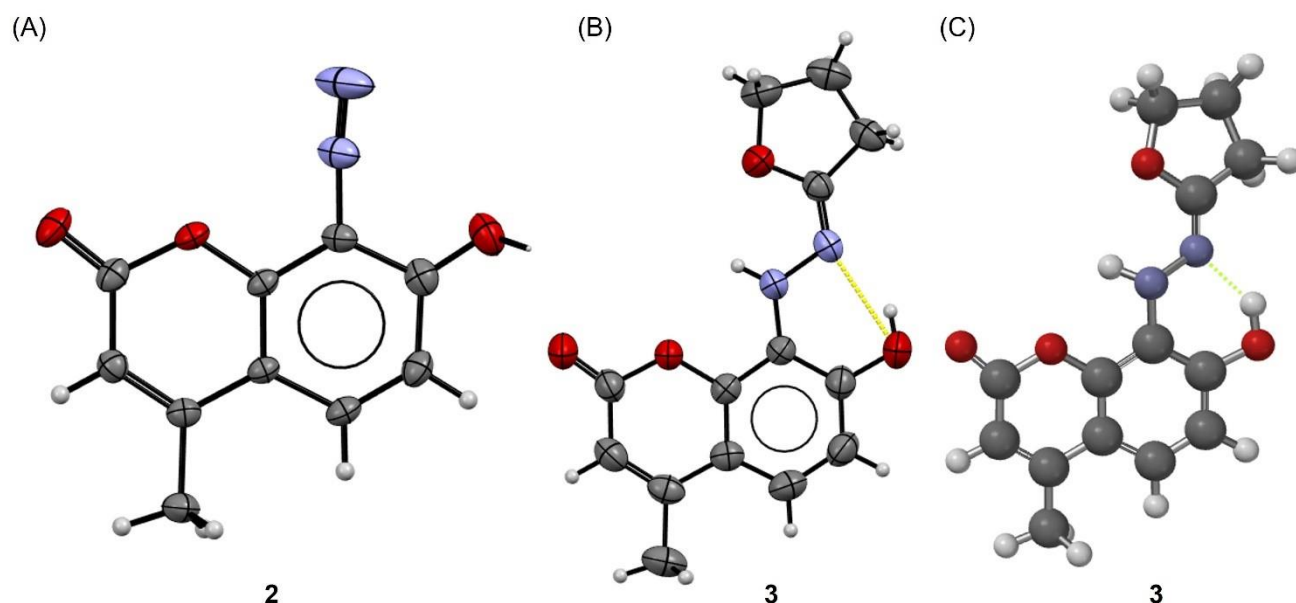
(A)   (B)   (C)

2   3   3

Figure 1. (A) Single-crystal X-ray structures of **2**; **(B)** Single-crystal X-ray structures of **3**; **(C)** computational molecular structure of **3** at PM3 level using Spartan '10 V1.10.

UV-Vis absorption assays

The chemosensing ability of **3** was investigated using UV-Vis spectral analysis in a water/acetonitrile (50/50) solvent system. **3** showed a spectral pattern in its unbound state with two absorption bands at 275 nm and 320 nm. We further explored the selectivity of **3** towards various metal ions that are mostly found in the water by mixing a solution of **3** with 0.5 molar equivalence of metal ions solutions of Ag^+, Na^+, Al^{3+}, Ca^{2+}, Ba^{2+}, Fe^{2+}, Fe^{3+}, Cr^{3+}, Hg^{2+}, Cu^{2+}, Co^{2+}, Cd^{2+}, Zn^{2+}, Li^+, Pb^{2+} and Ni^{2+} at room temperature. Interestingly, Cu^{2+}, Fe^{3+} and Hg^{2+} showed distinct spectral changes where a new absorption band formed at 300 nm upon adding any of these metal ions. The formation of the new peak indicates that **3** forms complexes with these metal ions. None of the other tested cations presented a notable change in the absorption spectra (Figure 2).

A systematic approach was carried out to determine the effect of competing cations on **3**-Cu^{2+}, **3**-Hg^{2+} and **3**-Fe^{3+} complexes (Figure 3). This was accomplished by adding 4.5 molar equivalence of metal ions to the solution of **3** before adding the same amount of Fe^{3+} to the recognition sensing system. The formation of the **3**-Fe^{3+} complex was not affected by the addition of competing metal ions compared to the **3**-Cu^{2+} and the **3**-Hg^{2+} complexes. This means that **3** is selective to Fe^{3+} in the presence of other metal ions, forming a more stable

complex with Fe^{3+} than any other competing cations. The chemosensor properties of **3** were further explored by examining its absorption spectra in the presence of different concentrations of Fe^{3+}. The gradual addition of Fe^{3+} resulted in a hyperchromic shift of the new absorption band at 300 nm. This further indicates that **3** forms a complex with Fe^{3+}. The complex's saturation point was attained after adding three molar equivalences of Fe^{3+}. Exactly two isosbestic points, at 280 nm and 325 nm, were observed in the absorption spectra of **3** with the addition of Fe^{3+} (Figure 4). This proves that there exist various stable complexes of **3**-Fe^{3+}.
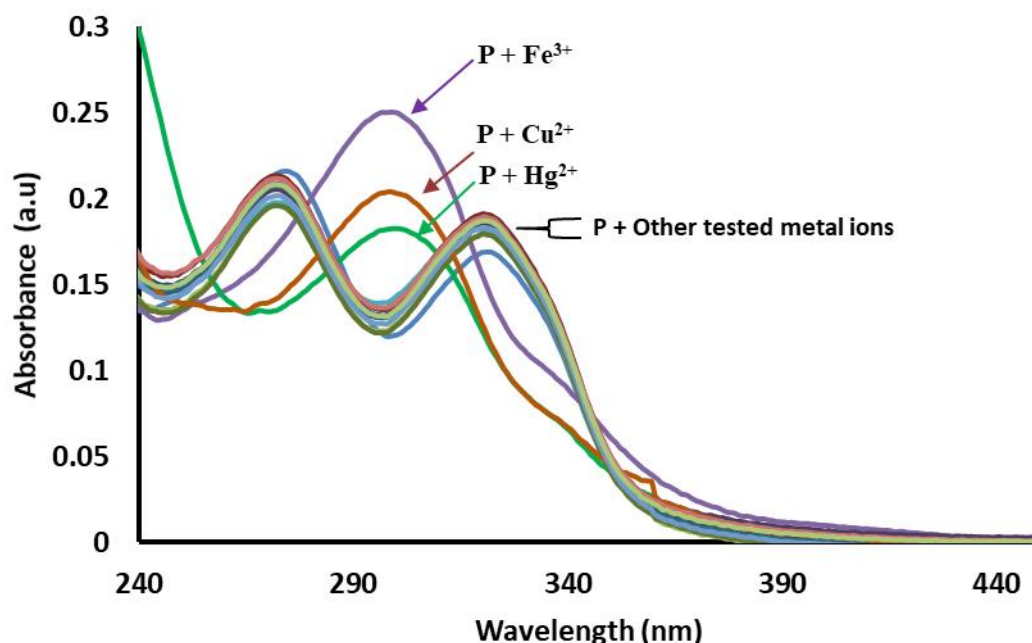

Figure 2. Absorption spectra of chemosensor **3** (1.53×10^{-4} mol/L) in the presence of 0.5 molar equivalence of different metal ions in water. Metal ion stock solution: 0.01M.
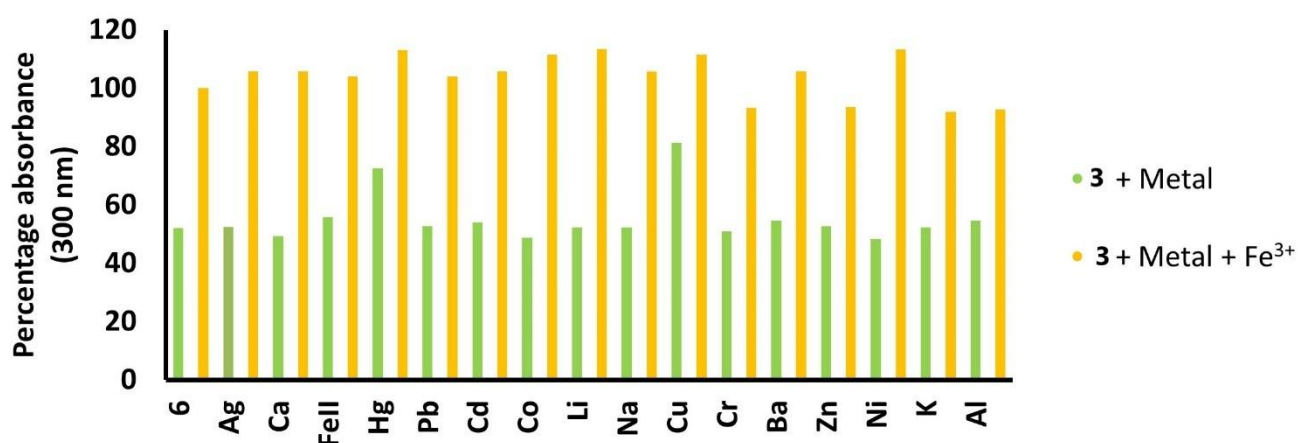

Figure 3. Absorption responses of **3** (1.53×10^{-5} M) upon addition of 4.5 molar equivalence of various metal ions (green bar) and addition of Fe^{3+} (mol eq) with other metal ions (mol eq) (orange bars). The experiments were performed in water, and the concentration of metal ion stock solutions was 0.01 M.
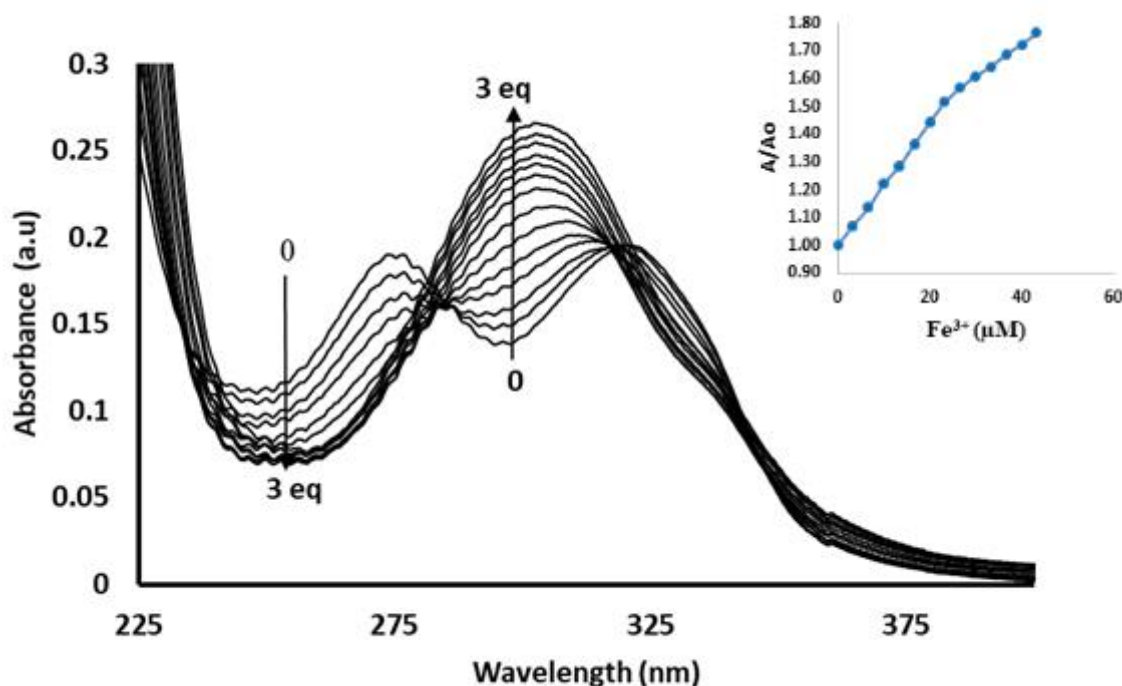
Figure 4. Absorption spectra of **3** (1.53×10^{-5} mol/L) in water-acetonitrile upon stepwise addition of Fe^{3+} aliquots ($0 - 4.33 \times 10^{-5}$ mol/L).

Emission spectroscopy

The metal cation chemosensing ability of **3** was investigated using emission spectral analysis in the water-acetonitrile solvent system. The selectivity of **3** towards metal ions was initially investigated by mixing it with metal ions solutions of Ag^+, Na^+, Ca^{2+}, Ba^{2+}, Fe^{2+}, Fe^{3+}, Cr^{3+}, Hg^{2+}, Cu^{2+}, Co^{2+}, Cd^{2+}, Zn^{2+}, Li^+, Pb^{2+} and Ni^{2+} at room temperature. There were no notable changes in the spectra of **3** when the metal was added except for Fe^{3+} (Figure 5). The interaction of Fe^{3+} with **3** caused a quenching in the emission of **3,** which indicates interaction. The competition experiments were conducted to assess the stability of the **3**-Fe^{3+} complex in the presence of other metal ions using fluorescence analysis.
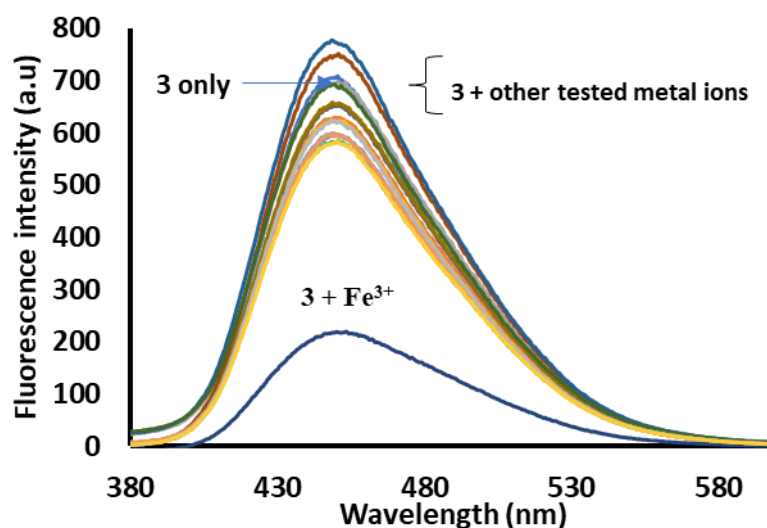
Figure 5. Emission spectra of chemosensor **3** (6.12×10^{-7} M) in the presence of the aliquot (8.33×10^{-4} M) of different metal ions. The experiments were conducted in water at an excitation wavelength of 320 nm.

To achieve this, 1.0 molar equivalence of metal ions were added to the solution of **3** before adding the equivalence of Fe^{3+} and monitoring the resultant fluorescence emission at 450 nm. In the presence of Ag^+, the quenching caused by Fe^{3+} could not be realized, whereas the opposite outcome was realized in the presence of other metal ions (Figure 6). This shows that the **3**-Ag^+ is a non-reversible complex, and thus Fe^{3+} complex can't form. However, **3** could still be used as a fluorometric chemosensor for Fe^{3+}.
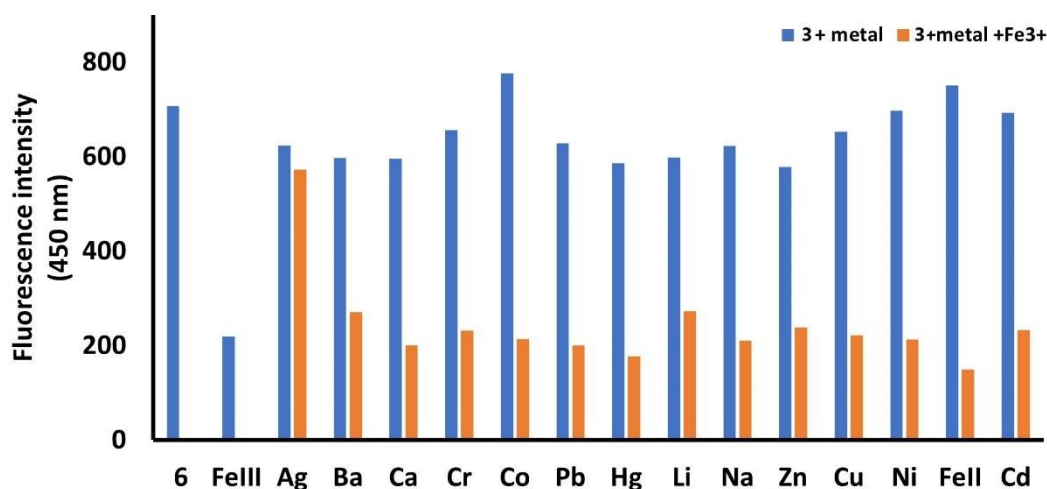

Figure 6. Fluorescence responses of **3** (6.12×10^{-4} M) upon the addition of various metal ions (8.33×10^{-4} M aliquot) (blue bar) and upon addition of Fe^{3+} (1.0 mol eq) with other metal ions (1.0 mol eq) (brown bars). The experiments were performed in water at an excitation wavelength of 320 nm, and the metal ion stock solutions had a concentration of 0.01 mol/L.

The titration experiments were conducted at room temperature at $\lambda_{excitation}$ = 320 nm, and a decrease in fluorescence intensity at 450 nm was observed with an increase in Fe^{3+} concentration (**Figure 7**). The saturation point of **3** was achieved after adding one molar equivalence of Fe^{3+}. The fluorescence quenching was due to the

heavy metal effects of Fe^{3+} ions [48]. The linearity in Fe^{3+} ion concentration was found in the $0 - 25$ µmol/L range with a correlation coefficient of $R^2 = 0.99$.
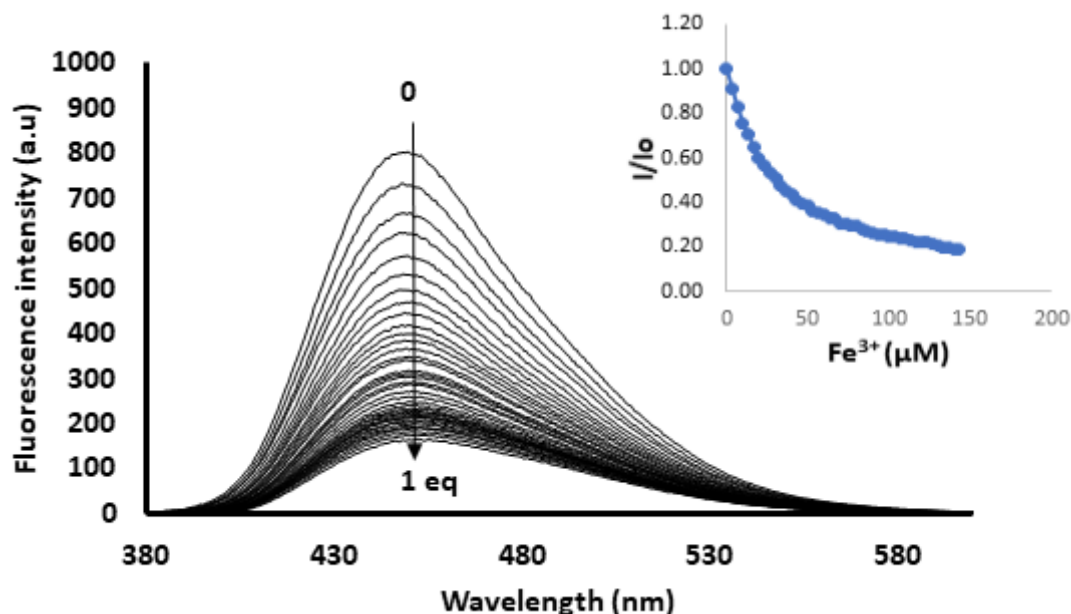

Figure 7. Emission spectra of chemosensor **3** (6.12×10^{-4} mol/L) in water/acetonitrile upon stepwise addition of Fe^{3+} aliquots ($0-1.4 \times 10^{-3}$ mol/L).

A Job's plot of **3** with Fe^{3+} was constructed to establish the stoichiometry relation of the **3**-Fe^{3+} complex using the continuous variation method [49]. The graph of emission intensity versus the molar fraction of Fe^{3+} at 450 nm indicates that the trend lines fitted to linear sections intersect exactly at 0.5 molar fraction (**Figure 8a**). This proposes a 1:1 stoichiometry of **3**-Fe^{3+} complexation. A plot of I_o/I against the molar concentration of Fe^{3+} is presented in **Figure 8b**, where I and I_o are the emission intensity in the presence of different concentrations of Fe^{3+} and the absence of Fe^{3+}, respectively. A linear Stern - Volmer calibration plot (Eq.1) with a correlation coefficient of 0.99 confirmed the presence of static quenching mode due to the formation of the **3**-Fe^{3+} complex. The association constant of 3.71×10^1 M^{-1} and the detection limit of 2.2 µM were evaluated graphically from a similar equation [50-51].

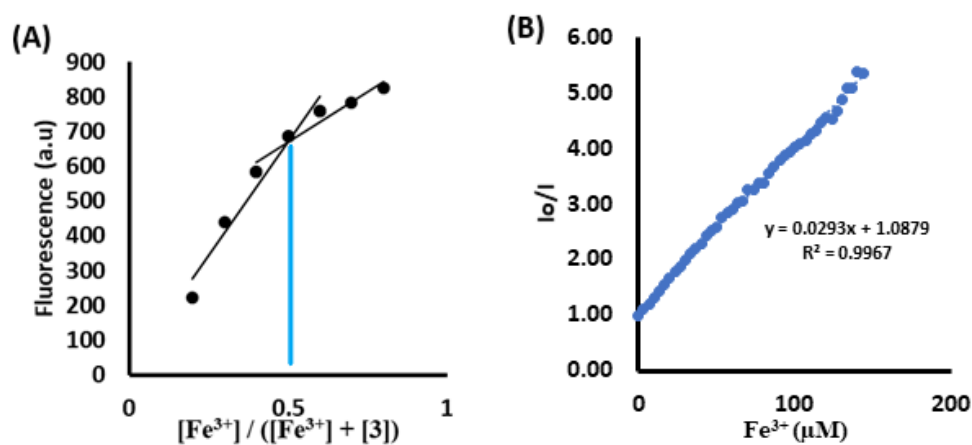**Figure 8**. (A) A Job's plot for **3**-Hg^{3+} binding in water/ acetonitrile with a constant total concentration of 6.12 × 10^{-7} mol/L. (B) A Stern – Volmer plot of I_o/I against $[Fe^{3+}]$.
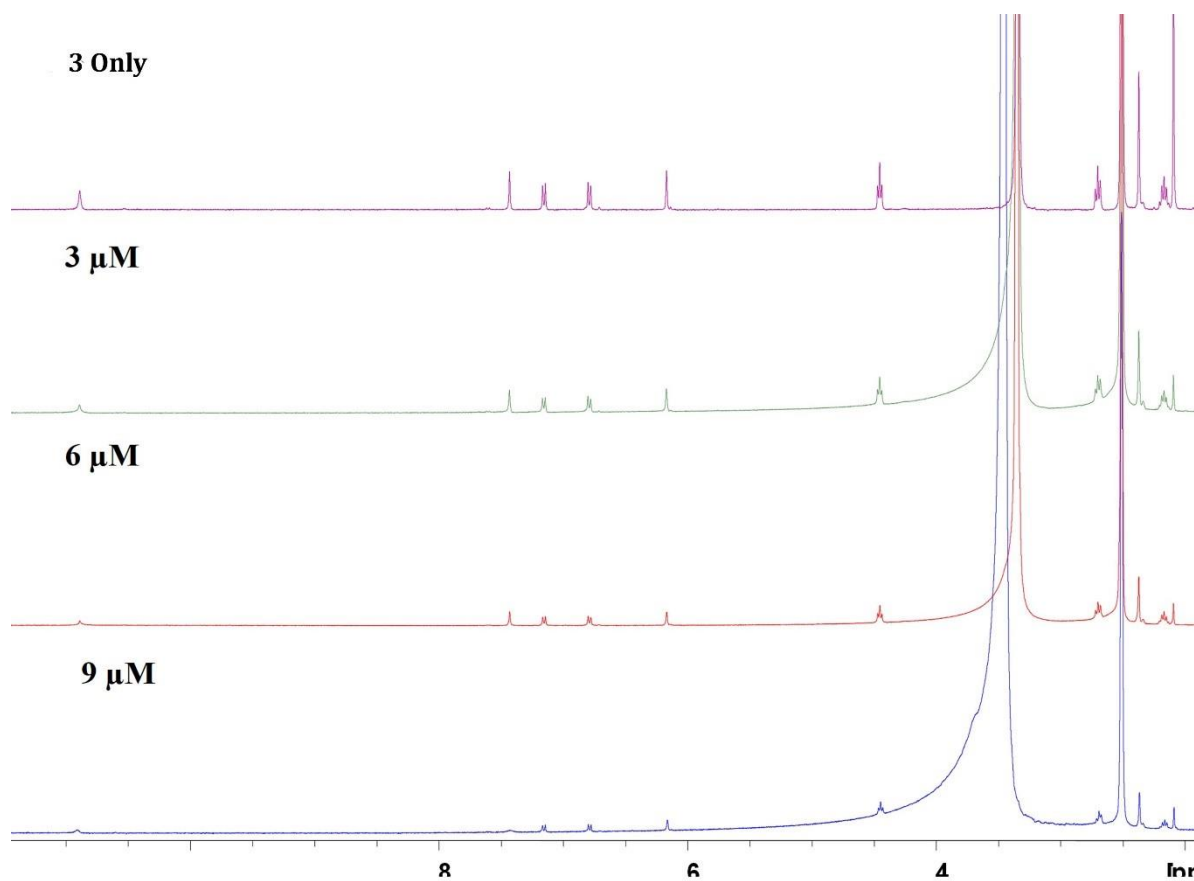
$$\frac{Io}{I} = 1 + Ksv\,[Fe^{3+}]$$

Equation .1

Figure 9. ^1H NMR signals of **3** with increasing amounts of Fe^{3+} in DMSO-d_6.

To understand the complexation mode of **3**-Fe^{3+}, ^1H NMR titration experiments using increasing amounts of Fe^{3+} were carried out. Stepwise addition of Fe^{3+} aliquots (3 µM) in deuterated dimethyl sulfoxide (DMSO-d_6) solution of **3** caused a decrease in intensity of all proton signals for the chemosensor**3** (Figure 9). This illustrates that Fe^{3+} interact with **3,** which causes a decrease in signal due to paramagnetism.

Molecular modelling studies were used to confirm the binding sites. The unbounded **3** shows higher electron density around the hydroxyl at position-7 and the hydrazone at position-8, and low electron density at carbonyl at position-2 and the methyl group at position-4 on the coumarin ring (**Figure 10A**). The electron-dense region can then take up a Lewis acid Fe^{3+} which can take up a lone pair of electrons, as illustrated in **Figure 10B**.
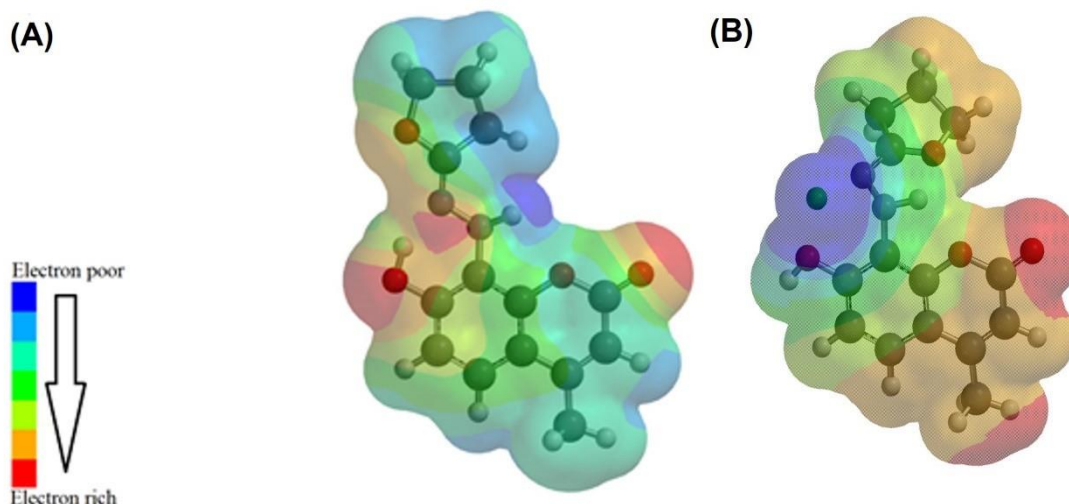

Figure 10. (A): Electron density of **3** and (B) **3**-Fe^{3+} complex at MMFF level using Spartan '10 V1.10.

The interaction between Fe^{3+} and the electron-dense region of **3** interrupts the charge transfers around the coumarin ring. The absorption and emission spectra analysis, Job's plot study and ^1H NMR titration experiment data of **3** all support the complexation with Fe^{3+}. It can be concluded that the complexation of Fe^{3+} with **3** involves the lone pairs of electrons on the hydroxyl and primary amine functionalities via a stable six-membered ring.

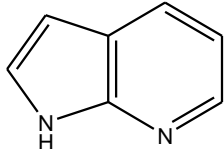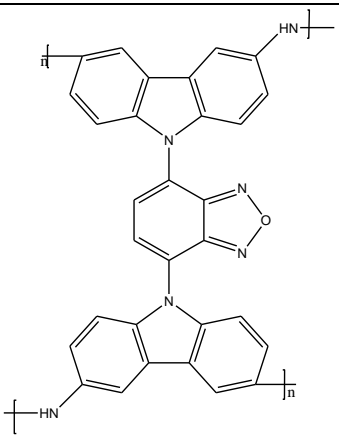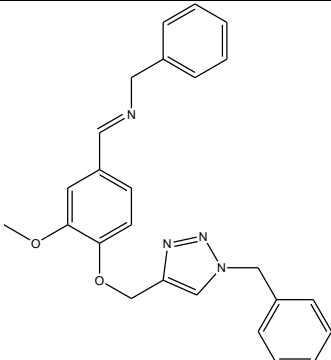**Table 1.** Comparative study on the proposed method and the existing fluorogenic Fe3$^+$ probes
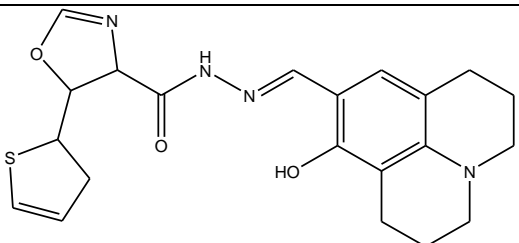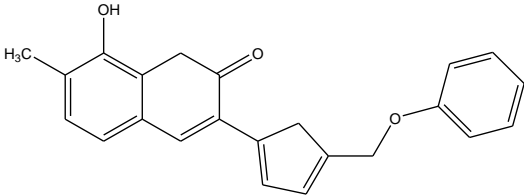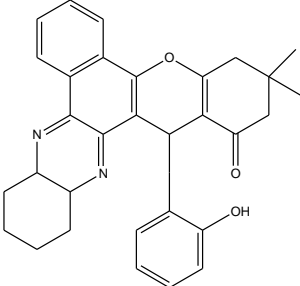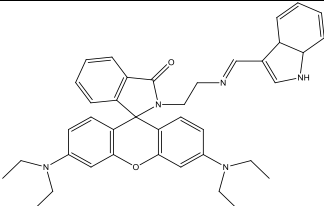
Proposed methods	LOD	Ka (M-1)	Ref.
3			
	0.46 µM	1.59×10^4 M^{-1}	52
	71.4 nM	1.49×10^1 M^{-1}	40
	1.3×10^{-7} M	2.6×10^4 M^{-1}	53
	8.45×10^{-9} M	-	54

Table 1. Continued

Proposed methods	LOD	Ka (M-1)	Ref.
3			
	1.4 µM	$3.3\times 10^4\,M^{-1}$	45
	$1.5 \times 10^{-5}\,M$	-	55
	$2.0 \times 10^{-5}\,M$	-	56

Conclusions

In summary, a new coumarin-based fluorescent chemosensor **3** incorporating a hydrazone was successfully synthesized through multiple-step syntheses. The addition of Fe^{3+} into acetonitrile/water solution of **3** resulted in the formation of a new absorption band at 300 nm and the quenching of the fluorescence. The competition studies of the **3**-Fe^{3+} complex showed that **3** could act as a highly sensitive fluorescent chemosensor for quantitative recognition of Fe^{3+} ions. The Job's plot analysis showed a possible 1: 1 binding ratio for the **3**-Fe^{3+} complex. The selectivity is greatly based on the involvement of the lone pairs of electrons on the hydroxyl and primary amine functionalities via stable six-membered rings, as illustrated by molecular modelling.

Experimental Section

General. All the reagents and solvents used to prepare the chemosensor were purchased from Sigma Aldrich, Merck and utilized without any purification. All derivatives of 8-amino-7-hydroxy-4-methyl-2*H*-chromen-2-one, **1**, were obtained according to the literature method [46]. The stock solution used for absorbance and fluorescence studies was obtained from pure solid samples of (E)-8-(2-(dihydrofuran-2(3H)-ylidene)hydrazinyl)-7-hydroxy-4-methyl-2H-chromen-2-one, **3**, which was dissolved in acetonitrile to yield a solution of 1.53×10^{-4} mol/L. Metal ion stock solutions (0.01 M) were prepared with pure water (Millipore water) (50ml) using sulphates salt for Fe^{2+}

and nitrate salts for all other metals (Ag^+, Na^+, Al^{3+}, Ca^{2+}, Ba^{2+}, Fe^{2+}, Fe^{3+}, Cr^{3+}, Hg^{2+}, Cu^{2+}, Co^{2+}, Cd^{2+}, Zn^{2+}, Li^+, Pb^{2+} and Ni^{2+}). The solutions of **3** were used in titration experiments conducted at room temperature using a 3 ml quartz cuvette.

Synthesis of Compound 1. Compound 1 was synthesized from literature proceedings[47] [32]. Yield 67%. Mp 112-127 °C. ^1H NMR (400 MHz, DMSO) δ 11.71 (s, 1H), 7.49 (d, *J* 8.3 Hz, 1H), 7.06 (d, *J* 8.4 Hz, 1H), 6.23 (s, 1H), 2.39 (s, 3H). ^{13}C (400 MHz, DMSO) 160.80, 154.56, 148.04, 141.75, 124.01, 112.89, 111.66, 110.39, 18.68. FT-IR V/cm 3040 (OH), 2380 (NH2), 1702 (C=O).

Synthesis of coumarin derivative 2. Coumarin derivative, 2, was synthesized by adding a solution mixture of 20 ml EtOH and 30 ml HCl (1M) to 1 (1.00 g, 5.70 mmol. The mixture was kept in ice until its temperature was below 5°C. $NaNO_2$ (2.00 g, 28.50 mmol) was added to the cooled mixture, and the mixture was stirred for 0.5 h. After a period of stirring, the resulting precipitate was filtered off, washed with water and dried under reduced pressure to afford the reddish-brown product 2 in 63% yield.

Synthesis of 3. Compound **2** (0,5 g), but-3-yn-2-ol (2 mol eq), Cu_2SO_4 (0.02g, 0.054 mmol), sodium ascorbate (0.03 g, 0.15 mmol), and PMDETA (0.03 g, 0.15 mmol) were added to tetrahydrofuran (THF) (20 mL) and stirred for 72 hours. THF was removed under reduced pressure, and the resultant crude product was purified by column chromatography over silica gel (Hexane: Ethyl acetate, 70:30) to yield compound **3** as a yellow solid in 75% yield. m.p. 125–130 °C. IR vmax (cm^{-1}): 3393 (O-H), 3302 (C-H), 2127 (N_2), 1683 (C = O), 1601 (C = C). ^1H NMR (500 MHz, DMSO-d) 10.88 (s, OH), δ 9.79 (s, 1H), 7.12 (d, *J* 7.5 Hz, 1H), 6.65 (d, *J* 7.5 Hz, 1H), 6.55 (q, *J* 0.9 Hz, 1H), 3.89 (d, *J* 2.2 Hz, 1H), 3.80 (d, *J* 2.2 Hz, 1H), 2.53 (t, *J* 7.1 Hz, 2H), 2.15 (t,3H), 1.54 – 1.45 (m, 2H). 13C NMR (125 MHz, DMSO-d) δ 168.45 , 162.92 , 155.55 , 151.15 , 137.18 , 123.78 , 122.87 , 121.96 , 113.55 , 113.26 , 97, 71.37, 29.81 , 21.59 , 21.31.

Measurements

The crude products were purified using Column Chromatography technique with silica gel of particle size 0.050 – 0.063 mm (70% ethyl acetate and 30% hexane). FT-IR spectra analysis to confirm compound functionalities was done using Opus software on a Perkin-Elmer FT-IR 180 spectrometer, and the ^1H NMR and ^{13}C NMR analyses were done on a Bruker Advance DPX 400 Spectrometer (400 MHz) in $CDCl_3$ or DMSO-d_6. NMR analyses were done at room temperature, and tetramethyl silane (TMS) was used as the internal reference. The Perkin Elmer Lambda 35 UV-Vis spectrometer and Perkin Elmer LS 45 spectrometer were used for recording UV-Vis and emission spectrum, respectively.

Acknowledgements

Supplementary Material

The copies of FT-IR, ^1H NMR, ^{13}C NMR spectra for compound **1, 2, 3** are available in the supplementary material file associated with this manuscript.

References

1. Carter, K.P.; Young, A.M.; Palmer, A.E. *Chem Rev*. **2014**, *114*, 4564-4601.
   https://doi.org/10.1021/cr400546e
2. Abbaspour, N.; Hurrell, R.; Kelishadi, R. *J. Res. Med. Sci*. **2014**, *19*, 164-174.
3. Grzeszczak, K.; Kwiatkowski, S.; Kosik-Bogacka, D. *Biomolecules* **2020**, *10,* 1-33.
   https://doi.org/10.3390/biom10081176
4. Ding, X.; Song, L.; Han, Y., *et al. Biomed. Res. Int*. **2019**, 2019.
   https://doi.org/10.1155/2019/8591631
5. Gordan, R.; Wongjaikam, S.; Gwathmey, J.K., *et al. Hear Fail Rev*. **2019**, *23*, 801-816.
   https://doi.org/10.1007/s10741-018-9700-5
6. Harper, R.M.J. *Lancet* **1949**, *254*(6591), 1202.
   https://doi.org/10.1016/S0140-6736(49)91856-5
7. Bayani Uttara, B.; Singh, A.V.; Zambani, P.; Mahajan, R.T. *Curr Neuropharmacalogy*. **2009**, *34,* 65-74.
   https://doi.org/10.2174/157015909787602823
8. Tchounwou, P.B.; Yedjou, C.G.; Patlolla, A.K.; Sutton, D.J. *Mol Clin Environ Toxicol*. **2012**, *101*, 33-164.
9. Masindi, V.; Muedi, K.L. *IntechOpen* **2018***, 7*, 1-20.
10. Jaishankar, M.; Tseten, T.; Anbalagan, N.; Mathew, B.B.; Beeregowda, K.N. *Interdiscip Toxicol*. **2014**, *7,* 60-72.
    https://doi.org/10.2478/intox-2014-0009
11. Corvalan, C.; Hales, S.; McMichael, A., *et al. World Heal Organ*. Published online **2005,** 1-59.
12. Galal-Gorchev, H. *WHO Guidelines for Drinking-Water Quality* Vol 11.; 1993.
13. Pivetta, T.; Masuri, S.; Cabiddu, M.G., *et al. New J Chem*. Published online **2019**, 32-38.
14. Liu Y.; Liang, P.; Guo, L. *Talanta* **2005**, *68*, 25-30.
    https://doi.org/10.1016/j.talanta.2005.04.035
15. Pourreza, N.; Ghanemi, K. *J. Hazard Mater*. **2009**, *161*, 982-987.
    https://doi.org/10.1016/j.jhazmat.2008.04.043
16. Al-Bedri, M.B.H.; Al-Jobori, S. *J. Radioanal. Nucl. Chem. Artic*. **1991**, *147*, 235-241.
    https://doi.org/10.1007/BF02040371
17. Guliyev, R. *Rational Design of Ratiometric Chemosensor Via Modulation of Energy Donor Efficiency*. 2008.
18. Achilefu, S. *Chem Rev*. **2010**, *110*, 2575-2578.
    https://doi.org/10.1021/cr1001113
19. Helaluddin, A.B.M.; Khalid, R.S.; Alaama, M.; Abbas, S.A. *Trop. J. Pharm. Res*. **2016**, *15*, 427-434.
    https://doi.org/10.4314/tjpr.v15i2.29
20. Peltomaa, R.; Glahn-Martínez, B.; Benito-Peña, E.; Moreno-Bondi, M.C. *Sensors (Basel)*. **2018**;*18*(12).
    https://doi.org/10.3390/s18124126
21. Dongare, P.R.; Gore, A.H. *ChemistrySelect*. 2021;6(23):5657-5669.
    https://doi.org/10.1002/slct.202101090
22. Damborský, P.; Švitel, J.; Katrlík, J. *Essays Biochem*. 2016;60(1):91-100.
    https://doi.org/10.1042/EBC20150010
23. Gupta, V.K.; Mergu, N.; Kumawat, L.K. *Sensors Actuators, B Chem*. 2016;223:101-113. Liu, Y.; Han, S.F., *et al. Sensors Actuators, B Chem*. **2017**;*244*, 914-921.
    https://doi.org/10.1016/j.snb.2017.01.074
24. Thevenot, D.; Toth, K.; Durst, R., *et al. Biosens Bioelectron*. Published online 2014.

25. Jeong, Y.; Yoon, J. *Inorganica Chim Acta*. **2012**, *381,* 2-14.
https://doi.org/10.1016/j.ica.2011.09.011

26. Ngororabanga, V.; Du Plessis, J.; Mama, N. Sensors **2017**, *17*, 1980.
https://doi.org/10.3390/s17091980

27. Wheelock, C.E. *J. Am. Chem. Soc*. **1959**, *81,* 1348-1352.
https://doi.org/10.1021/ja01515a021

28. Chua, M.H.; Shah, K.W.; Zhou, H.; Xu, J. *Molecules* **2019**, *24,* 2711.
https://doi.org/10.3390/molecules24152711

29. Wang, L.; Li, W.T.; Qu, W.J. *et al. J. Braz. Chem. Soc*. **2018**, *29*, 1563-1569.
https://doi.org/10.21577/0103-5053.20180030

30. Fan, G.; Yang, L.; Chen, Z. *Front. Chem. Sci. Eng*. **2014**, *8,* 405-417.
https://doi.org/10.1007/s11705-014-1445-7

31. Quang, D.T.; Kim, J.S. *Chem. Rev*. **2010**, *110*, 6280-6301.
https://doi.org/10.1021/cr100154p

32. Wei, T.B.; Zhang, P.; Shi, B.B., *et al. Dye Pigment*. **2013**, *97*, 297-302.
https://doi.org/10.1016/j.dyepig.2012.12.025

33. Luo, A.; Wang, H.; Wang, Y.; Huang, Q.; Zhang, Q. *Spectrochim Acta - Part A Mol Biomol Spectrosc*. **2016**, *168,* 37-44.
https://doi.org/10.1016/j.saa.2016.05.048

34. Liu, Y.; Duan, W.; Song, W.; *et al. ACS Appl. Mater. Interfaces* **2017**, *9*, 12663-12672.
https://doi.org/10.1021/acsami.6b15746

35. Xie, Z.; Sun, X.; Jiao, J.; Xin, X. *Colloids Surfaces A Physicochem. Eng. Asp*. **2017**, *529*(May), 38-44.
https://doi.org/10.1016/j.colsurfa.2017.05.069

36. Zhou, M.; Guo, J.; Yang, C. *Sensors Actuators, B Chem*. **2018**, *264,* 52-58.
https://doi.org/10.1016/j.snb.2018.02.119

37. Yang, G.; Wan, X.; Su, Y.; Zeng, X.; Tang, J. *J. Mater. Chem. A*. **2016**, *4,*12841-12849.
https://doi.org/10.1039/C6TA05943K

38. Ngororabanga, J.M.V.; Moyo, C.; Hosten, E.; Mama, N.; Tshentu, Z.R. *Anal. Methods*. **2019**, *11*, 3857-3865.
https://doi.org/10.1039/C9AY00463G

39. Ngororabanga, J.M.V.; Tshentu, Z.R.; Mama, N. *New J. Chem*. **2019**, *43*, 12168-12177.
https://doi.org/10.1039/C9NJ01366K

40. Ngororabanga, J.M.V.; Tshentu, Z.R.; Mama, N. *J. Fluoresc*. **2020**, *30*, 985-997.
https://doi.org/10.1007/s10895-020-02542-x

41. 42. Ngororabanga, J.M.V.; Moyo, C.B.; Tshentu, Z.R. *Spectrochim Acta - Part A Mol Biomol Spectrosc*. **2020**, *242*, 118651.
https://doi.org/10.1016/j.saa.2020.118651

42. Ngororabanga, J.M.V.; Du Plessis, J.; Mama, N. Fluorescent polymer incorporating triazolyl coumarin units for Cu2+ detection via planarization of Ict-based fluorophore. *Sensors (Switzerland)*. 2017;17(9).
https://doi.org/10.3390/s17091980

43. Naimhwaka J, Uahengo V. A naphthoquinone based colorimetric probe for real-time naked eye detection of biologically important anions including cyanide ions in tap water: Experimental and theoretical studies. *RSC Adv*. 2019;9(65):37926-37938. doi:10.1039/c9ra06116a
https://doi.org/10.1039/C9RA06116A

44. Mama, N.; Battison, A. *Arkivoc*. **2020**,(v), 59 - 84…

https://doi.org/10.24820/ark.5550190.p011.283

45. Sahoo, S.S.; Shukla, S.; Nandy, S.; Sahoo, H.B. *Eur J Exp Biol*. **2012**, *2*, 899-908.

46. Sivakumar K, Xie F, Cash BM, Long S, Barnhill HN, Wang Q. *Org. Lett*. **2004**, *6*, 4603-4606.
https://doi.org/10.24820/ark.5550190.p011.283

47. Da En; Yuan Guo; Bo-Ting Chen; Biao Dong; Meng-Jiao Peng RSC Adv. Published online 2014:248-253.
https://doi.org/10.1039/C3RA44843F

48. Renny, J.S;, Tomasevich, L.L.; Tallmadge, E.H.; Collum, D.B. *Angew Chemie - Int Ed*. **2013**, *52,* 11998-12013.
https://doi.org/10.1002/anie.201304157

49. Wahba, M.E.K.; El-Enany, N.; Belal, F. *Anal Methods* **2015**, *7*, 10445-10451.
https://doi.org/10.1039/C3AY42093K

50. Rivera-Figueroa, A.M.; Ramazan, K.A. Finlayson-Pitts, B.J. *J. Chem. Educ*. **2004**, *81*, 242-245.
https://doi.org/10.1021/ed081p242

51. Mehata, M.S.; Aneesha. *Photochem Photobiol Sci*. Published online **2023**:1505-1516.
https://doi.org/10.1007/s43630-023-00393-6

52. George, N.; Singh, G.; Singh, R. et al. *Polyhedron*. **2023**, 242.
https://doi.org/10.1016/j.poly.2023.116496

53. Liu, Y.; Cui, H.; Wei, K.; *et al. Spectrochim Acta - Part A Mol. Biomol. Spectrosc*. **2023**, *292*(December 2022).
https://doi.org/10.1016/j.saa.2023.122376

54. Harichandran, G.; Parameswari, P.; Shanmugam, P. *Sensors Actuators B Chem*. **2018**, *272*(May), 252-263.
https://doi.org/10.1016/j.snb.2018.05.134

55. Samanta, S.; Ray, T.; Haque, F.; Das G. *J. Lumin*. **2016**, *171,* 13-18.
https://doi.org/10.1016/j.jlumin.2015.10.043